ISSN 1392 - 1207. MECHANIKA. 2010. Nr.2(82)

Influence of structure and mechanical properties for cyclic fracture rates of cast iron

M. K. Leonavičius*, A. Krenevičius, J. Bacevičius*****
**Vilnius Gediminas Technical University, Saulėtekio 11, 10223 Vilnius, Lithuania, E-mail: mindaugas.leonavicius@vgtu.lt*
***Vilnius Gediminas Technical University, Saulėtekio. 11, 10223 Vilnius, Lithuania, E-mail: kron@vgtu.lt*
****Vilnius Gediminas Technical University, Saulėtekio 11, 10223 Vilnius, Lithuania, E-mail: jonas.bacevicius@gmail.com*

1. Introduction

There is a lot of information about the resistance of cast iron to cyclic loads when a number of cycles exceeds 10^8 [1-7]. Some consistent patterns and peculiarities were observed during experiment data analysis to be used for the purpose of applying the gained results for the calculation of designed durability. Current paper presents the already accomplished achievements as well as the analysis of further investigations by determining the limits of the fatigue crack growth threshold at very low speeds.

The durability of such elements exceeds 25 years, and the number N of loading cycles enters the giga-cycle range $N > 10^8$ cycles. The casting of hull details from grade iron and gears from spherical graphite iron and the following heat treatment are connected with certain pronounced problems. To achieve the required microstructure, it is necessary to apply the heat treatment normalization, which has to guarantee a microstructural change throughout all the large volume. During the normalization process it is necessary to obtain microstructures with a pearlite matrix, but usually there remains some part of ferrite, which is mild and undesirable. The ferrite matrix around graphite nodules produces a negative influence on the mechanical properties: it reduces hardness and strength of the structure.

Austempered ductile iron (ADI) is a spheroid graphite iron produced by using special stages of heat treatment, which comprise the production of a ductile cast iron, austenisation (at about 800-1000°C), followed by quenching of the temperature (at about 250-450°C), suitable for the final stage, and the isothermal transformation (austempering) of some of the austenitic matrix to other phases before subsequent cooling till it reaches 20°C. By varying the heat treatment parameters and changing the obtained microstructure, the mechanical properties can alter significantly (σ_u = 800-1600 MPa). Using both the metallurgical and technological means, composition of the cast iron is optimised, the intergrain surfaces are cleaned from impurities. While the casting is held at the austempering temperature, the nucleation and growth of **a**ccrular ferrite occurs, accompanied by the transition of carbon into austenite. The resulting microstructure, known as "Ausferrite", gives ADI its special attributes. Ausferrite exhibits twice the strength of a given level of ductility, if compared to the pearlitic, feritic or martensitic structures formed by conventional heat treatments.

2. Resistance to cyclic fracture

Stress intensity factor K and load cycle asymmetric factor $R = K_{min}/K_{max}$ are the parameters defining the state of stress and strain in the top crack of the elastic body and determining the crack's propagation consistent pattern in cyclic fracture mechanics. Parameter K places the state and size of load, shape and size of the crack and the body. Therefore, during consistent patterns research of the fatigue fracture, it is enough to use the fatigue crack growth rate da/dN dependence either on stress-intensity factor range $\Delta K = (1-R)\,K_{max}$ either on maximum stress-intensity factor K_{max}

$$\frac{da}{dN} = V = f\left(K_{max},\, K_{min}/K_{max},\, C,\, m\right) \tag{1}$$

where a is the propagating fatigue crack depth, N is the number of load cycles, C and m are constants.

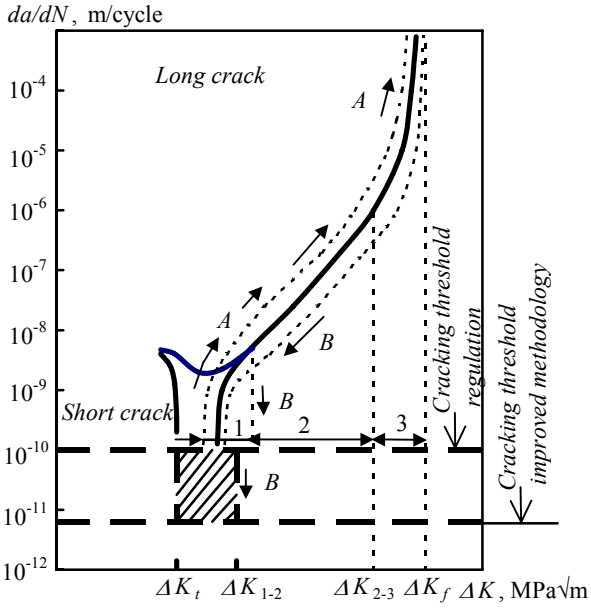

Fig. 1 Cyclic fracture process diagram: A – kinetic fatigue diagram; B – crack growth versus stress intensity factor range

The typical kinetic fatigue diagram, presented in logarithmic scale, is shown in Fig. 1. The diagram is limited by the stress intensity factor value ΔK_{th} (fatigue crack growth threshold) on the left. The crack does not propagate below this factor or its very slow propagation is taking to be acceptable. Critical cyclic stress intensity factor K_{fc} limits the diagram on the right side. Rude fracture of specimen takes place after above mentioned value has been reached. Usually kinetic fatigue diagram is charted by testing

specimen either through the special eccentrically-loaded tension or bending. It is possible to test constructive elements. The experiment begins by making crack growth as shown by pointer *A* in Fig. 1. The microstructure of the material, stress and indicators of ambient impact make a big influence in sector 1, the so-called low speed sector. It is accepted that the crack does not grow when the speed is below than 10^{-10} m/cycle in standard, regulating cyclic strength tests. The influence of microstructure decreases in sector 2 (medium speeds sector), but the load and ambient indicators gain strength. The steepness the line in the sector 2 (connected with different *m* values in well-known Paris equation) the faster the crack's growth becomes in current material. There is a big influence of the body thickness, microstructure and the main stress value in the final fracture (high fatigue speeds) sector 3 [2, 8, 9].

The big quantity of microscopic points of plastic strain appears in spheroidal cast iron before the main crack formation. The following points become the focuses of microscopic fatigue cracks. This phenomenon is caused by graphite cores, microstructure defects and internal voids. Under the cyclic load, when the maximum stress is lower than cyclic durability, the fatigue cracks originate, but do not propagate beyond the particular length. Such nonpropagatable cracks show that the cyclic strength is not a limit of stress, under which the fatigue cracks do not form, but indicate the material's ability to resist the propagation of the originated cracks. When a crack originates in the graphite core environment of spheroidal graphite cast iron it is possible to consider that the stress in the core is small in comparison with the stress in the matrix. The stress and the limit stress under which fatigue cracks originate but do not propagate, is 2-3% less than cyclic durability limit [1, 2].

Various graphs present the propagation of short cracks in the typically kinetic fatigue diagram (Fig. 1). The experimental analysis is insufficient for the determination of further crack propagation taking place in this range.

Such a limit may not be sufficient if the durability of the design equipment exceeds 25 years. Therefore the fatigue strength research is relevant to the limit approaching to 10^{-12} m/cycle which corresponds to its longer service life (25-50 years) [3].

If parameter ΔK_{th} is used for cyclic strength and durability calculations, then the stress intensity factor and cracks growth rate diagrams are drawn, but the kinetic fatigue diagram not. In the latter case the crack growth is suspended as shown by the marker *B* in Fig. 1.

The data about the resistance to cyclic load of different cast irons when ΔK_{th} dimensions are at $v = 5 \cdot 10^{-12}$ m /cycle are presented in the works [3-5]. Larger results dispersal than at $v = 1 \cdot 10^{-10}$ m /cycle have been observed as shown in Fig. 1 (lined sector of diagram).

3. Structure and mechanical properties

For the experiment four as cast iron and four normalized cast iron plates of all kinds have been prepared. The chemical compositions of the investigated irons are presented in Table 1.

The chemical compositions, produced the setting and the casting procedures were carried out in the foundry, and differ from the well known similar cast irons used in the USA, Germany, Australia and Finland.

Table 1

Chemical composition

Cast iron	C	Si	Mn	Ni	Mo	Cu	Cr
	%						
1	3.64	1.75	0.870	0.497	0.520	0.518	0.062
2	4.96	1.17	0.083	0.680	0.190	1.010	-
3	3.50	2.24	0.353	2.920	0.407	0.800	0.407
4	3.61	2.22	0.351	1.968	0.395	0.805	0.395

During heat treatment, the investigated plates were settled at various sites of the furnace beside large sized details. Microstructure of the cast iron 1 is shown in Fig. 2, a. Graphite is present in the shape of flakes of different size; the structural matrix is represented by ferrite-pearlite. At some points the spherical graphite gets formed. Microstructure of the normalized cast iron 1 is shown in Fig. 2, b. The microstructure is fine-grained, the graphite is spherical, and the base of the microstructure shows pearlite with a small amount of ferrite.

The microstructure of the cast iron 2 is shown in Fig. 3, a. It consists of flakes of different size and spherical graphite. The matrix is pearlite with irregularly situated ferrite, although sometimes bainite were observed. The microstructure after normalizing is shown in Fig. 3, b. It consists of spherical graphite, small-grained pearlite, bainite and ferrite. As we can see, normalizing makes the microstructure uniform and fine. The obtained nodular graphite is of a similar size.

Microstructure of the cast iron 3 and 4 is shown in Fig. 4. The matrix is bainite. Graphite is spheroidal and of various sizes, anomalous shape (shape of flakes) also can be noticed.

From all the plates, tension specimens are fabricated. Mechanical properties are defined; they are presented in Table 2.

CT specimens have been produced from all the plate-materials-altogether six types of specimens characterised by different mechanical properties (Table 2). Cylindrical tensile specimens taken from some broken specimens for the specification of mechanical properties have been produced.

Hardness of the cast iron 1 is 250-277 BHN, of the normalized is 228-256 BHN, and hardness of the cast iron 2 is 289-311 BHN, and of the normalized one is 290-311 BHN. Hardness of the cast iron 3 is 318-323 BHN and

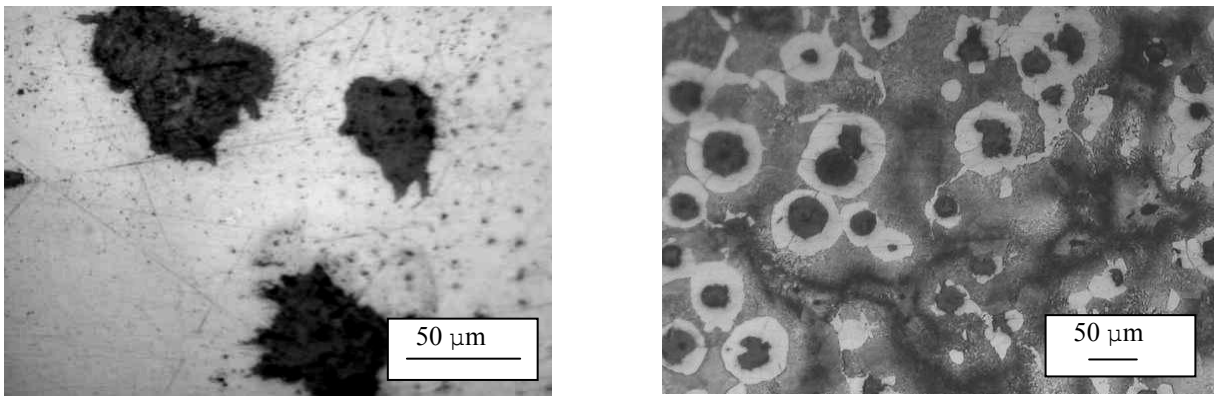

a b

Fig. 2 Microstructure of cast iron 1: a – as cast, b – normalized

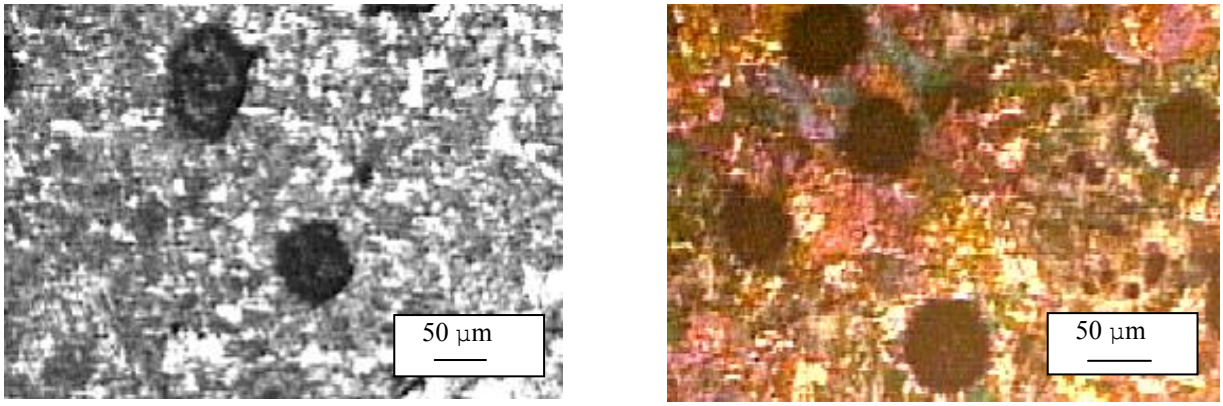

a b

Fig. 3 Microstructure of cast iron 2: a – as cast, b – normalized

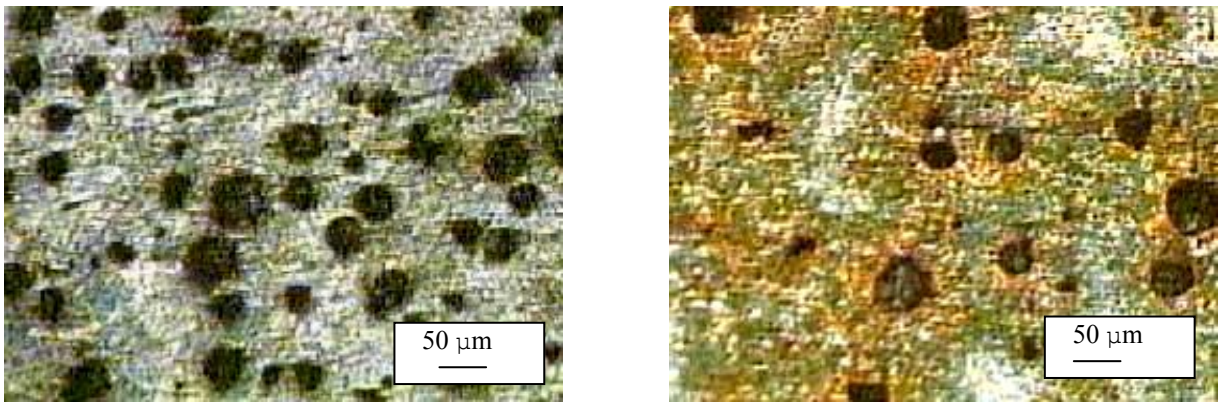

a b

Fig. 4 Microstructure of cast iron 3 and 4: a – ADI-1, b – ADI-2

Table 2

Mechanical properties

Cast iron		Yield strength	Ultimate tensile strength	Elongation
		$R_{p0.2}$, MPa	R_m, MPa	A_5, %
1	As cast	443 to 503	622 to 671	1.80 to 2.43
	Normalized	454 to 467	684 to 727	6.13 to 10.30
2	As cast	630 to 634	863 to 933	3.70 to 6.70
	Normalized	607 to 621	862 to 882	3.60 to 4.00
3	ADI-1	834 to 845	1034 to 1077	8.90 to 11.20
4	ADI-2	699 to 705	918 to 952	4.30 to 5.70

299-311 BHN for cast iron 4. As we can see, in the process of heat treatment, the hardness changes slightly. The heat treatment process consists of normalization and annealing, performed when following the requirements set technological processes for of the real construction.

4. Analysis of experimental results

In order to obtain the cracking threshold, standard test method (ASTM E-647-00) has been modified and applied for the experimental research of eccentrically loaded specimens (CT). The proposed experiment implementation and the postprocessing modification of the resulting data enables researchers to estimate the void's influence on the cracking threshold.

The total number of the cycles for austempered ductile iron specimens varies from 11.4 to 20.3 million cycles, for pearlitic cast iron – from 10.0 to 19.6 million cycles.

One of the basic quantitative crack resistance indices is the cracking threshold limit stress intensity factor range ΔK_{th}. The performed research is remarkable due to the fact that the obtained values of the limit stress intensity factor range are obtained at lower crack propagation rates than the standard test method requires. The propagation rates are decreased to $v \approx 5 \cdot 10^{-12}$ m/cycle in order to obtain the cracking threshold corresponding to a longer lifetime of the parts. To be able to calculate the stress intensity factor, the following formula is applied

$$K = \frac{F}{B\sqrt{W}} f\left(\frac{a}{W}\right) \tag{2}$$

where $f(x) = \left[(2+\lambda)/(1-\lambda)^{2/3}\varphi(\lambda), \lambda = a/W\right]$,

$$\varphi(\lambda) = 0.866 + 4.64\lambda - 13.32\lambda^2 + 14.72\lambda^3 - 5.6\lambda^4$$

and F is tension force, B is specimen width, W is specimen base length, a is crack length.

The front of the crack propagation is different in each specimen because of different reasons (mainly due to the inhomogenity of the structure and its porosity).

The crack growth rate versus stress intensity factor range diagrams have been following the experimental research results of all 6 sorts CT specimens made of cast iron. Fig. 5 presents the cast iron 1 diagram: as cast iron – 8 specimens, normalized – 8 specimens. There are data of the cast iron 2 in Fig. 6: as cast iron – 4 specimens, normalized – 4 specimens. Fig. 7 presents data of the cast iron 3 and 4 iron: ADI-1 – 5 specimens, ADI-2 – 4 specimens.

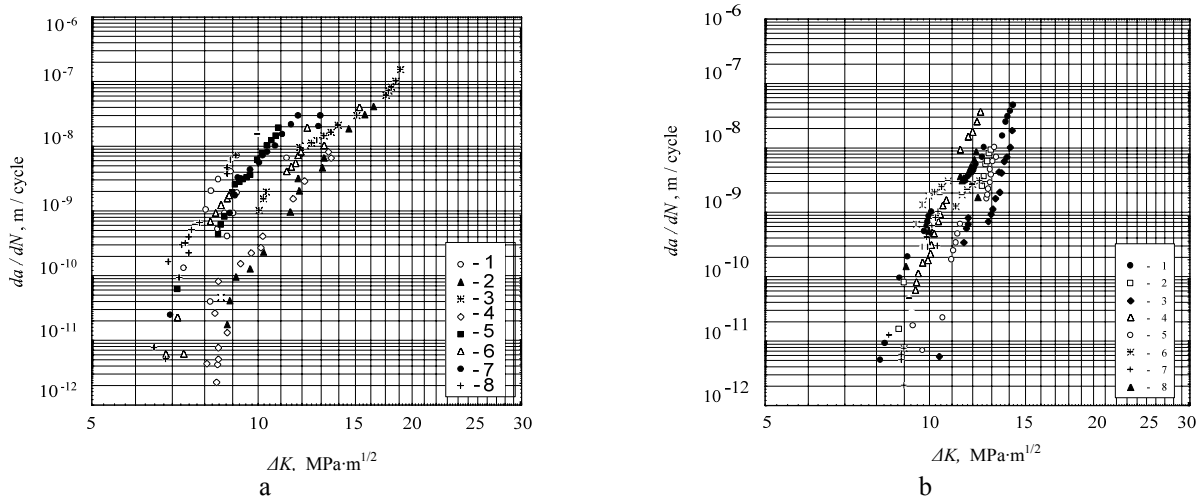

a b

Fig. 5 Crack growth rate versus stress intensity factor range of cast iron 1: a – as cast, b – normalized

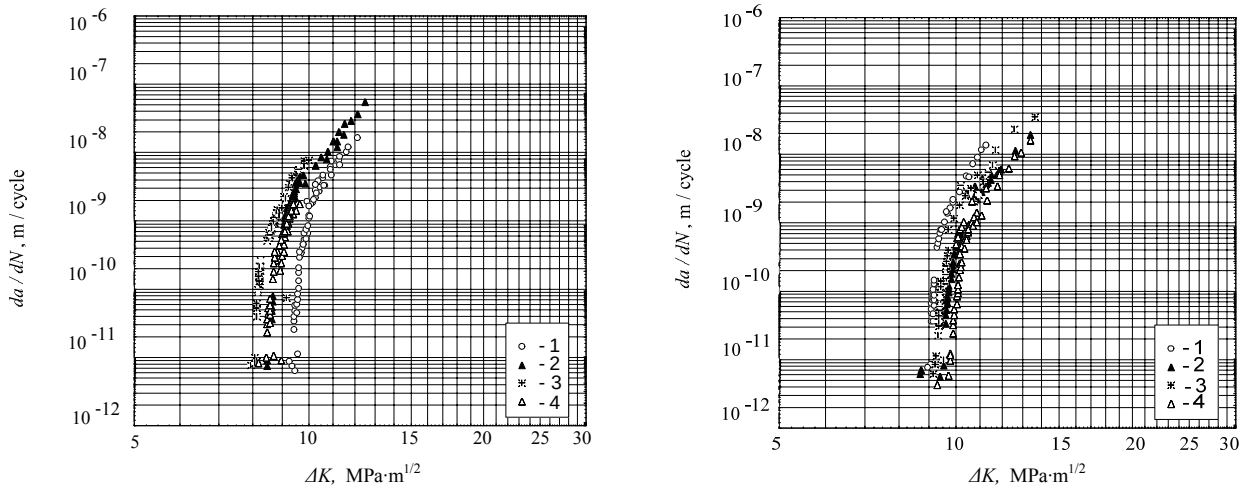

a b

Fig. 6 Crack growth rate versus stress intensity factor range of cast iron 2: a – as cast, b – normalized

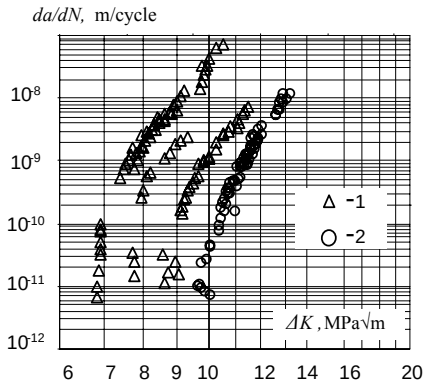

Fig. 7 Crack growth rate versus stress intensity factor range of cast iron 3 and 4: 1 – ADI-1, 2 – ADI-2

During the experimental research, it has been observed that ΔK_{th} rely in crack's depth for some specimens. Additional tests have been performed for CT specimen of cast iron 2. ΔK_{th} versus v diagram is presented in Fig. 8. Fracture of CT specimen with fixed crack's depth 16.2; 18.5; 21.1; 25.2; 29.2 mm is shown in Fig. 9. If $\Delta K_{th} \approx$ ≈ 9.8 MPa$\sqrt{\text{m}}$ at the speed $v = 10^{-10}$ m /cycle, when approaching to speed $v = 5 \cdot 10^{-12}$ m /cycle - $\Delta K_{th} \approx 8.7$-9.9 MPa$\sqrt{\text{m}}$. There we observe different ΔK_{th} values at different crack's depth in the diagram.

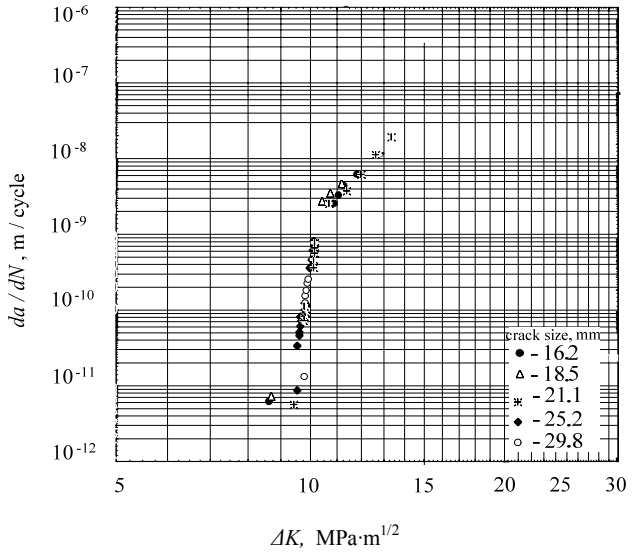

Fig. 8 Crack growth rate versus stress intensity factor range

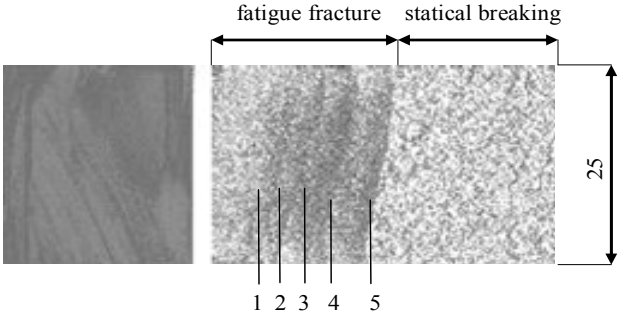

Fig. 9 Fracture of CT specimen: 1 to 5 are crack-stopping tracks

Additional tests have been performed with CT specimens of ADI-2 cast iron. Width of the specimen was reduced to 12.5 mm in order to stabilise the crack's front e. g. to reduce its obliquity.

It is observable that ΔK_{th} values practically coincide at different depth of crack 15.4 mm; 22.5 mm and 24.7 mm for specimen ADI2-a1. Measured ΔK_{th} values at 18 mm, 26.4 mm and 33.6 mm depth of coincide also with specimen ADI2-a2. Dispersal of ΔK_{th} results is small – 8.2-8.4 MPa$\sqrt{\text{m}}$. The obtained values are close to minimal ΔK_{th} presented in Fig. 7.

5. Static fracture of compact specimens

After crack growth rates versus stress intensity factor range have been designed (Figs. 5-8), compact specimens with cracks were used to measure the plane strain fracture toughness. For this purpose, the static fracture tests have been performed.

The measurement of plane strain fracture toughness K_{1C} value is not always possible, but the measured data are noteworthy and could be used to evaluate the material's suitability for production of structural elements (fracture strength). It is auxiliary information for the calculation of structural elements following the main criterion - threshold stress intensity range ΔK_{th}.

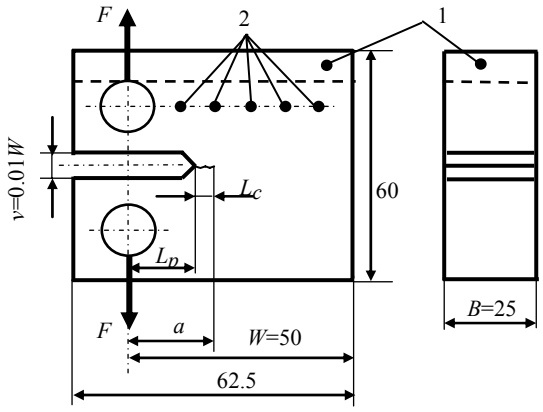

Fig. 10 Load layout of compact specimen

When performing static fracture of CT specimen's (Fig. 10), the measuring system records the value of alternate force F and crack's opening. Hardness of each CT specimen has been additionally measured (at points 2). Tensile specimens have been produced from cut part 1 and indicators of mechanical properties have been revised. After the analysis of crack's opening diagram, the value of force F_Q received becomes possible to use when calculating K_{1C} or K_C. Works [1, 9] present three types of crack's opening diagrams and introduce the appropriate calculating technique. Fig. 11 presents the static fracture diagram of cast iron 1 specimen. The diagram is specific because of the topical force maximum which is considered F_Q value. This force is suitable for the calculation of plane strain fracture toughness K_{1C} value if there is an adequate chart point between the lines 0-a and 0-b and $F_Q > F_5$, the same as $F_{max}/F_Q \leq 1.1$. If the topical force maximum is on the right side of the line 0-b, it is possible to calculate K_C value only when using the measured F_Q value.

The calculating value of crack's length L_{cr}, is de-

termined by three measurements of fracture (at centre and sides of specimen). The average of these three measurements is L_{cr} calculating value. K_{1C} can be calculated only if the following conditions are met

$$\frac{\left|\left(L_0 + L_{cr,max}\right) - \left(L_0 - L_{cr,min}\right)\right|}{\left(L_0 + L_{pl,min}\right)} \cdot 100\% < 10\% \tag{3}$$

where $L_{cr,max}$ and $L_{cr,min}$ are maximum and minimum values of measured crack's length.

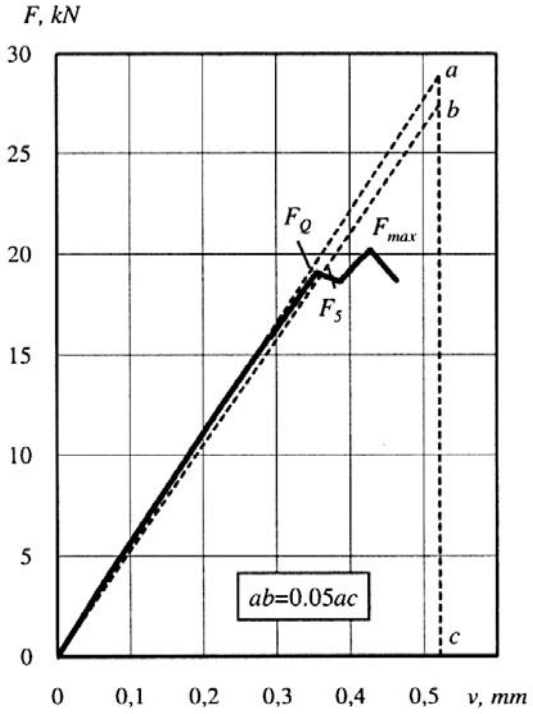

Fig. 11 Static fracture diagram of cast iron 1 compact specimen

When calculating value L_{cr} the determined following condition should be verified

$$0{,}45 \le a \le 0{,}55W \tag{4}$$

This condition indicates the limits where the formula for the calculating of stress intensity rate K_1 for compact specimen may be used

$$K_1 = \frac{F}{B\sqrt{W}} f\left(\frac{a}{W}\right) \tag{5}$$

where

$$f\left(\frac{a}{W}\right) = \frac{2 + \frac{a}{W}}{\left(1 - \frac{a}{W}\right)^{3/2}} \left[\begin{array}{l} 0.886 + 4.64\left(\frac{a}{W}\right) - \\ -13.32\left(\frac{a}{W}\right)^2 + 14.72\left(\frac{a}{W}\right)^3 - \\ -5.6\left(\frac{a}{W}\right)^4 \end{array}\right] \tag{6}$$

The above-mentioned conditions should be verified when using calculated value and other known or determined indicators of the specimen and material. If the conditions are satisfied – the calculated K_C value is plane strain fracture toughness indicator K_{1C}. If one of the conditions does not match, the calculated K_C is the critical stress intensity factor only (in literature it is sometimes mentioned as the conditional critical stress intensity factor K_C) [8-12].

The critical stress intensity factor K_Q is determined for CT specimens of cast and normalized iron 1, 2 and 3, 4. When one of the mentioned conditions does not match the requirements the fracture toughness is determined if all the conditions correspond. The results are presented in Table 3.

Table 3

Critical stress intensity factors of different types of cast iron

Cast iron		K_C, MPa $\sqrt{\text{m}}$
1	as cast	28.7-38.8
	normalized	38.1-40.3
2	as cast	2.0-30.9
	normalized	28.4-32.6
3	ADI-1	60.8-78
4	ADI-2	59.5-67

According to experimental research the crack growth rate versus stress-intensity factor range has been designed (Fig. 12).

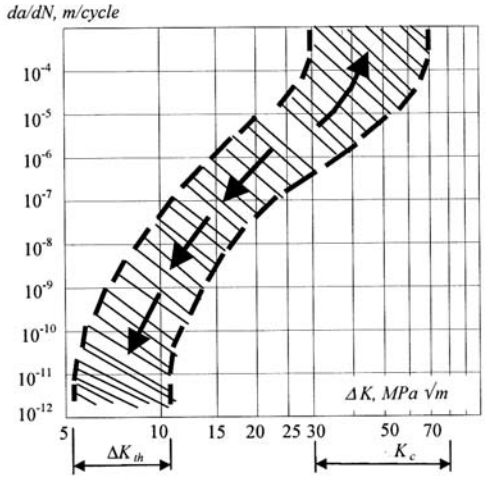

Fig. 12 Crack growth rate versus stress intensity factor range at cast iron: 1, 2 and 3, 4

The picture presents critical stress intensity factor K_C. The current part of the diagram includes all the static break results of CT specimens (K_{1C} – plane strain fracture toughness, K_C – critical stress intensity for static failure).

5. Conclusions

1. The analysis of the experimental analytical research of critical stress intensity factors (cracking threshold and fracture toughness) for 6 types of cast iron has been performed. Mechanical properties and the structure have been measured.

2. The regulated methodology for critical stress intensity factors (cracking threshold) measurement has been changed in so that the results would be used for the increase of the durability of big size cast iron parts.

3. The experimental research analysis shows that the cracking threshold of the same cast iron differs in quite a wide range while decreasing the cracking speed from $1 \cdot 10^{-10}$ m /cycle to $5 \cdot 10^{-12}$ m /cycle.

4. The conditional critical stress intensity factor which was determined for CT specimens with crack could be used as auxiliary criteria when calculating cyclic strength and confirming the material suitability for the structure elements if the calculation methodology is based on the main criteria – cyclic cracking threshold.

References

1. **Ritchie, R.O.** Mechanisms of fatigue-crack propagation in ductile and brittle solids.-International Journal of Fracture, 1999, p.55-83.
2. **Matvienko, Yu.G.** Fracture Mechanics Models and Criterion.-Moscow: PhysMatLit, 2006.-328p. (in Russian).
3. **Leonavičius, M.K., Petraitis, G., Šukšta, M., Svalbonas, V.** Strenght of mills and crushers equipment materials subjected to gigacycle loading.-Journal of Civil Engineering and Management.-Vilnius: Technika, 2006, v.12, No.2, p.135-141.
4. **Leonavičius, M.K., Petraitis, G., Krenevičius, A., Šukšta, M., Stupak, S.** Investigation of high-cycle fatigue of cast iron with porous layer near threshold ΔK_{th}.-Kovove Materials: Metallic Materials.-Bratislava: Kovové materially, 2005, v.43, p.348-357.
5. **Leonavičius, M.K., Krenevičius, A., Stupak, S., Petraitis, G., Šukšta, M., Bazaras, Ž.** The strenght of as cast iron and normalized cast iron subjected to cyclic loading.-Stroiniški vestnik.-Ljubljana: Association of Mechanical Engineers of Slovenia, 2006, v.52, No.9, p.558-567.
6. **Dorazil, E.** High Strength Austempered Ductile Cast Iron.-Prague: Ellis Harwood, 1991.-244p.
7. **Rajnovic, D., Eric, O., Sidjanin, L.** Microstructure and fracture of cooper alloyed ADI material.-Proceedings of ECF 16 th European Conference of Fracture Failure Analysis of Nano and Engineering Materials and Structures, 3-7 July, 2006, Alexandroupolis, Greece.
8. **Broek, D.** The Practical Use of Fracture Mechanics.-Dorsdrecht-Boston-London: Kluwer Academic Publishers, 1989.-426p.
9. **Žiliukas, A.** Strenght and Failure Criteria. Monograph. -Kaunas: Technologija, 2006.-208p. (in Lithuanian).
10. **Daunys, M., Česnavičius, R**. Low cycle stress strain curves and fatigue under tension-compression and torsion. -Mechanika. -Kaunas: Technologija, 2009, Nr.6(80), p.5-11.
11. **Daunys, M., Bazaras, Z., Timofeev, B.T.** Low cycle fatigue of materials in nuclear industry.-Mechanika. -Kaunas: Technologija, 2008, Nr.5(73), p.12-18.
12. **Bražėnas, A., Vaičiulis, D**. Low cycle stress strain curves and fatigue under tension-compression and torsion. -Mechanika. -Kaunas: Technologija, 2009, Nr.6(80), p.5-11.

M. K. Leonavičius, A. Krenevičius, J. Bacevičius

STRUKTŪROS IR MECHANINIŲ SAVYBIŲ ĮTAKA KETAUS CIKLINIO IRIMO RODIKLIAMS

R e z i u m ė

Straipsnyje apibendrinami atlikti darbai ir analizuojami papildomi tyrimai, kuriais siekiama nustatyti pleišėjimo slenksčio ribas, esant labai mažiems plyšio plitimo greičiams ($5 \cdot 10^{-12}$ m /ciklą). Šiomis sąlygomis plyšio plitimui didelę įtaką turi ketaus mikrostruktūra ir mechaninės savybės. Pastebėta didesnė eksperimentinių rezultatų sklaida ir nestabilus plyšio plitimas. Gauti duomenys panaudoti konstrukcijų elementų ilgaamžiškumo skaičiavimui.

M. K. Leonavičius, A. Krenevičius, J. Bacevičius

INFLUENCE OF STRUCTURE AND MECHANICAL PROPERTIES FOR CYCLIC FRACTURE RATES OF CAST IRON

S u m m a r y

This paper presents the study and perform analysis of additional research by measuring limits of cracking threshold at very low speeds ($5 \cdot 10^{-12}$ m /cycle). The microstructure and mechanical properties of cast iron make big influence on crack propagation. Big dispersal of experimental research data unstable propagation of the crack was noticed. The obtained data were used for the calculation of durability of structural elements.

M. K. Ляонавичюс, А. Креневичюс, Й. Бацевичюс

ВЛИЯНИЕ СТРУКТУРЫ И МЕХАНИЧЕСКИХ СВОЙСТВ НА ПОКАЗАТЕЛИ ЦИКЛИЧЕСКОГО РАЗРУШЕНИЯ ЧУГУНА

Р е з ю м е

На основании выполненных работ и дополнительных исследований анализируется предел трещиностойкости при малых скоростях ($5 \cdot 10^{-12}$ м /цикл) распространения трещины. В этом диапазоне большое влияние имеет микроструктура и механические свойства чугуна. Замечены разброс экспериментальных данных и нестабильное распространение трещины. Полученные данные способствуют расчету конструктивных элементов на долговечность.

Received February 15, 2010
Accepted April 10, 2010

DOI: 10.5755/j02.mech.15513